SUPPORTING INFORMATION: Composition and electronic structure of Mn_3O_4 and Co_3O_4 cathodes in zinc/air batteries: a DFT study

Fernanda Juarez and Hui Yin
Institute of Theoretical Chemistry, Ulm University, 89069 Ulm, Germany

Axel Groß*
Institute of Theoretical Chemistry, Ulm University, 89069 Ulm, Germany and
Helmholtz Institute Ulm (HIU), Electrochemical Energy Storage, 89069 Ulm, Germany

S1. THEORETICAL BACKGROUND

A. Ab initio Thermodynamics applied to the Solid-Gas Interface

The thermodynamic stability of a surface can be described by the Gibbs energy of formation $\Delta\gamma$, defined by

$$\Delta\gamma = \frac{1}{2A_S}\Big(g_{surf} - \sum_i n_i\tilde{\mu}_i(T,p,U)\Big), \tag{S1}$$

where g_{surf} is the Gibbs energy of the surface, A_S is its area, and $\tilde{\mu}_i$ and n_i are the chemical potentials and number of the species, respectively. For each of these species, the reservoir will depend on the nature of the interface that it is being represented. In the present work we consider the following situations: 1) oxide slabs in contact with gaseous reservoirs, and 2) the same slabs embedded in a solution that contains the reservoir species.

For the purpose of obtaining expressions of the chemical potentials we followed the approach of Scheffler *et al* in their seminal paper [S1]. Firstly, the chemical potentials of oxygen and hydrogen μ_O and μ_H were written using their molecular species (O_2 and H_2). Subsequently, all the terms depending on temperature and pressure were collected in $\Delta\mu_O$ and $\Delta\mu_H$ (e.g. $\mu_X(T,p) = 1/2 g_{X_2} + \Delta\mu_X(T,p)$). Secondly, we assumed the thermodynamic equilibrium between the surface and the underlying bulk oxide, which act as reservoir of the metal atoms. Therefore and according to the Gibbs-Duhem equation, the chemical potential of the metal atoms μ_M is: $g_{M_xO_y} = x\mu_M + y\mu_O$. The final expression of the Gibbs energy of formation in the gas phase is

$$\Delta\gamma^{GAS} = \frac{1}{2A_S}\Big(\Delta G^{GAS}_{form} - \Big(n_O - \frac{4}{3}n_M\Big)\Delta\mu_O - n_H\Delta\mu_H\Big), \tag{S2}$$

where the energy of formation is equal to

$$\Delta G^{GAS}_{form} = E_{surf} - \frac{1}{3}n_M E_{bulk} - \frac{n_H}{2}\left(E_{H_2} + ZPE_{H_2} - TS_{H_2}\right) - \Big(n_O - \frac{4}{3}n_M\Big)\left(E_{O_2} + ZPE_{O_2} - TS_{O_2}\right)/2\,. \tag{S3}$$

and E_i, ZPE_i, and S_i are the total energy, the zero-point-energy and the entropy of the corresponding systems. The phase diagrams were later constructed using the systems with the lowest Gibbs energy of formation $\Delta\gamma^{GAS}$ at each value of $\Delta\mu_O$ and $\Delta\mu_H$.

As it was already pointed out in [S1], the availability of the reservoir species can be restricted by other relevant reactions occurring in the simulated system. Then, the values of the chemical potentials cannot be unlimited varied. A general restriction is that the chemical potential $\mu_i(T,p)$ of the species i must be lower than the chemical potential of its standard state, beyond which only the standard form is thermodynamically stable. In the case of oxygen and hydrogen, their standard states are the diatomic molecules O_2 and H_2, respectively. Hence, their upper limit is: $\Delta\mu_i \leq 0$ [S1]. A suitable lower boundary of μ_O in any type of oxides is the decomposition of the oxide into pure metal and molecular oxygen. This reaction only occurs if the chemical potential of the metal μ_M is larger than the Gibbs free energy of the pure metal bulk g_M, that is its standard state. Because O and M are in thermodynamic equilibrium, the restriction in the chemical potential of one becomes a limit for the other one and thus the lower bound of $\Delta\mu_O$ becomes the heat of formation $\Delta G_{form}(M_xO_y)$ per O atom.

* axel.gross@uni-ulm.de

B. Computational Hydrogen Electrode applied to the Solid-Liquid Electrochemical Interface

As we mentioned before, our goal is to simulate the conditions of an operating battery where pH and potential of the electrode are the main variables of control. In this situation the reservoirs of species are different than in the gas phase, specifically: H^+, M^{2+}, HMO_2^- ions, and H_2O. Following the same approach than in [S2], we obtained the expressions of the electrochemical potentials in terms that we could calculate through DFT.

We begin with the chemical potential of H^+. Protons and electrons in the solution are in equilibrium with the hydrogen molecule, through the redox half-reaction: $2H^+_{(auk)} + 2e^-_{(auk)} \rightleftharpoons H_{2\,(g)}$, hence the following equation is established

$$\tilde{\mu}_{\mathrm{H^+}} + \tilde{\mu}_{e^-} = \frac{1}{2}\mu_{\mathrm{H_2}} - a_{SHE} - k_{\mathrm{B}} \ln(10)\mathrm{pH}, \tag{S4}$$

where e is the charge of the electron, and U_{SHE} is the electrode potential in the saturated hydrogen scale (SHE). All the terms related with the electrode potential and pH were regrouped in

$$\Delta\tilde{\mu}_{\mathrm{H^+}} = -eU_{SHE} - k_{\mathrm{B}}T \ln(10)\mathrm{pH}\,. \tag{S5}$$

The expression of the electrochemical potential of the acidic ion M^{2+} in equilibrium with the other species present in the solution was found using the half-reaction: $3M^{2+}_{(aq)} + 4H_2O_{(l)} \rightleftharpoons M_3O_{4\,(s)} + 8H^+_{(aq)} + 2e^-_{(aq)}$. Then its electrochemical potential is given by

$$\tilde{\mu}_{\mathrm{M^{2+}}} + \frac{2}{3}\tilde{\mu}_{e^-} = \frac{1}{3}\mu_{\mathrm{M_3O_4}} - \frac{4}{3}\mu_{\mathrm{H_2O}} + \frac{8}{3}\tilde{\mu}_{\mathrm{H^+}}, \tag{S6}$$

The last equation can be converted to include the electrode potential among others quantities. Using the Nernst equation, assuming standard conditions for the pressure of H_2 and replacing $\tilde{\mu}_{\mathrm{H^+}}$ according to Eq. S4, it gives

$$\tilde{\mu}_{\mathrm{M^{2+}}} + \frac{2}{3}\tilde{\mu}_{e^-} = \frac{1}{3}\mu_{\mathrm{M_3O_4}} - \frac{4}{3}\mu_{\mathrm{H_2O}} + \frac{8}{3}\tilde{\mu}_{\mathrm{H^+}} + \frac{2}{3}e\left(U^0_{\mathrm{H^{2+}/M_3O_4}} - U_{SHE}\right) - \frac{8}{3}k_{\mathrm{B}}T\ln(10)\mathrm{pH} - k_{\mathrm{B}}T\ln(\alpha_{\mathrm{H^{2+}}}), \tag{S7}$$

where $\alpha_{\mathrm{H^{2+}}}$ is the activity of the M^{2+} ion in the solution. The terms related to the experimental parameters were collected in

$$\Delta\tilde{\mu}_{\mathrm{M^{2+}}} = \frac{2}{3}e\left(U^0_{\mathrm{M^{2+}/M_3O_4}} - U_{SHE}\right) - \frac{8}{3}k_{\mathrm{B}}T\ln(10)\mathrm{pH} - k_{\mathrm{B}}T\ln(\alpha_{\mathrm{M^{2+}}})\,. \tag{S8}$$

In both Eqs. S5 and S8, the electrode potential U_{SHE} appears. By combining these equations, a relation between the electrochemical potentials of H^+ and M^{2+} can be derived in which the electrode potential is no longer explictly included:

$$\Delta\tilde{\mu}_{\mathrm{M^{2+}}} = \frac{2}{3}eU^0_{\mathrm{M^{2+}/M_3O_4}} + \frac{2}{3}\Delta\tilde{\mu}_{\mathrm{H^+}} - 2k_{\mathrm{B}}Tln(10)\mathrm{pH} - k_{\mathrm{B}}Tln(\alpha_{\mathrm{M^{2+}}})\,. \tag{S9}$$

Following the same procedure, the electrochemical potential of the alkaline ion HMO_2^- is equal to

$$\tilde{\mu}_{\mathrm{HMO_2^-}} + \frac{2}{3}\tilde{\mu}_{e^-} = \frac{1}{3}\mu_{\mathrm{M_3O_4}} + \frac{2}{3}\mu_{\mathrm{H_2}O} - \frac{1}{3}\tilde{\mu}_{\mathrm{H^+}} + \frac{2}{3}e\left(U^0_{\mathrm{HMO_2^-/M_3O_4}} - U_{SHE}\right) + \frac{1}{3}k_{\mathrm{B}}T\ln(10)\mathrm{pH} - k_{\mathrm{B}}T\ln(\alpha_{\mathrm{HMO_2^-}}), \tag{S10}$$

where all the experimental variables were accumulated in $\Delta\tilde{\mu}_{\mathrm{HMO_2^-}}$. The ions in the solution are in acid/base equilibrium, kept through the reaction

$$\mathrm{H^{2+}_{(aq)}} + 2\mathrm{H_2O_{(l)}} \rightleftharpoons \mathrm{HMO^-_{2\,(aq)}} + 3\mathrm{H^+_{(aq)}} \tag{S11}$$

As a consequence, their molar fractions and electrochemical potentials are not independent from each other. For simplicity, in the following we will refer to the change in the electrochemical potential of M^{2+} or HMO_2^- as one quantity: $\Delta\tilde{\mu}_{\mathrm{M}}$. This simplification does not change the expression of the Gibbs energy of formation but it cannot be applied to the Pourbaix diagrams.

By replacing Eqns. S4, S7, and S10 in Eq. S1, a new expression of the Gibbs energy of formation was obtained

$$\Delta\gamma^{AQ} = \frac{1}{2A_S}\left(\Delta G^{AQ}_{form} - n_{\mathrm{M}}\Delta\tilde{\mu}_{\mathrm{M}} - \left(n_{\mathrm{H}} - 2\left(n_{\mathrm{O}} - \frac{4}{3}n_{\mathrm{M}}\right)\right)\Delta\tilde{\mu}_{\mathrm{H^+}}\right), \tag{S12}$$

where the corresponding energy of formation is equal to

$$\Delta G^{AQ}_{form} = E_{surf} - \frac{1}{3} n_{\mathrm{M}} E_{bulk} - \left(n_{\mathrm{H}} - 2 \left(n_{\mathrm{O}} - \frac{4}{3} n_{\mathrm{M}} \right) \right) \left(E_{\mathrm{H_2}} + \mathrm{ZPE}_{\mathrm{H_2}} - T S_{\mathrm{H_2}} \right) / 2 - \left(n_{\mathrm{O}} - \frac{4}{3} n_{\mathrm{M}} \right) \left(E_{\mathrm{H_2O}} + ZPE_{\mathrm{H_2O}} - T S_{\mathrm{H_2O}} \right) . \quad \text{(S13)}$$

In this case and different to the gas phase, the Gibbs energy of formation and phase diagrams are functions of $\Delta\tilde{\mu}_M$ and $\Delta\tilde{\mu}_{\mathrm{H^+}}$, which are mutually dependent on the pH and electrode potential. The Pourbaix diagrams were constructed by explicitly writing these relationship in Eq. S12.

Once again, the upper bound of the electrochemical potential of H^+ is the chemical potential of H_2, for which: $\Delta\tilde{\mu}_{\mathrm{H^+}} = 0$. However, in this case it corresponds to the electrolysis of water in the cathode at potential: $U_{SHE} = -k_{\mathrm{B}}T/e \ \ln(10)\mathrm{pH}$. Furthermore, the decomposition of water into O_2 at the other electrode establishes the lower limit of $\tilde{\mu}_{\mathrm{H^+}}$. This is because hydrons and hydroxyls ions in the solution are in thermodynamic equilibrium. The lower limit in the electrochemical potential becomes: $\Delta\tilde{\mu}_{\mathrm{H^+}} = -1.23$ eV at potential: $U_{SHE} = 1.23\,\mathrm{V} - k_{\mathrm{B}}T/e \ \ln(10)\mathrm{pH}$.

The electrochemical potential of the metal ions can be limited by the formation of many different types of oxides. We only consider the dissolution of the bulk M_3O_4 oxide to form M^{2+} or HMO_2^- ions. Other processes were not impose as limits because we studied explicitly the oxidation and reduction of the oxide via hydroxylation and hydrogenation of the surface.

According to experimental Pourbaix diagrams, to avoid the reduction of M_3O_4 to 2+ ions the electrode potential must be:

$$U_{SHE} \geq U_{\mathrm{M^{2+}/M_3O_4}} = U^0_{\mathrm{M^{2+}/M_3O_4}} - \frac{k_{\mathrm{B}}T}{e} \left(4 \ \ln(10)\,\mathrm{pH} + \frac{3}{2} \ln(\alpha_{\mathrm{M^{2+}}}) \right) \quad \text{(S14)}$$

in acidic media, or in alkaline solution:

$$U_{SHE} \geq U_{\mathrm{HMO_2^-/M_3O_4}} = U^0_{\mathrm{HMO_2^-/M_3O_4}} - \frac{k_{\mathrm{B}}T}{e} \left(\frac{1}{2} \ln(10)\,\mathrm{pH} + \frac{3}{2} \ln(\alpha_{\mathrm{HMO_2^-}}) \right) . \quad \text{(S15)}$$

The lower bound of the potential corresponds to an upper limit of the electrochemical potential: $\Delta\tilde{\mu}_{\mathrm{M}} \leq 0$, beyond which the ions are the only stable state.

[S1] K. Reuter and M. Scheffler, Composition, structure, and stability of RuO_2 (110) as a function of oxygen pressure, Phys. Rev. B **65**, 035406 (2001).

[S2] F. Gossenberger, F. Juarez, and A. Groß, Sulfate, bisulfate, and hydrogen co-adsorption on Pt(111) and Au(111) in an electrochemical environment, Front. Chem. **8**, 634 (2020).

S2. FIGURES

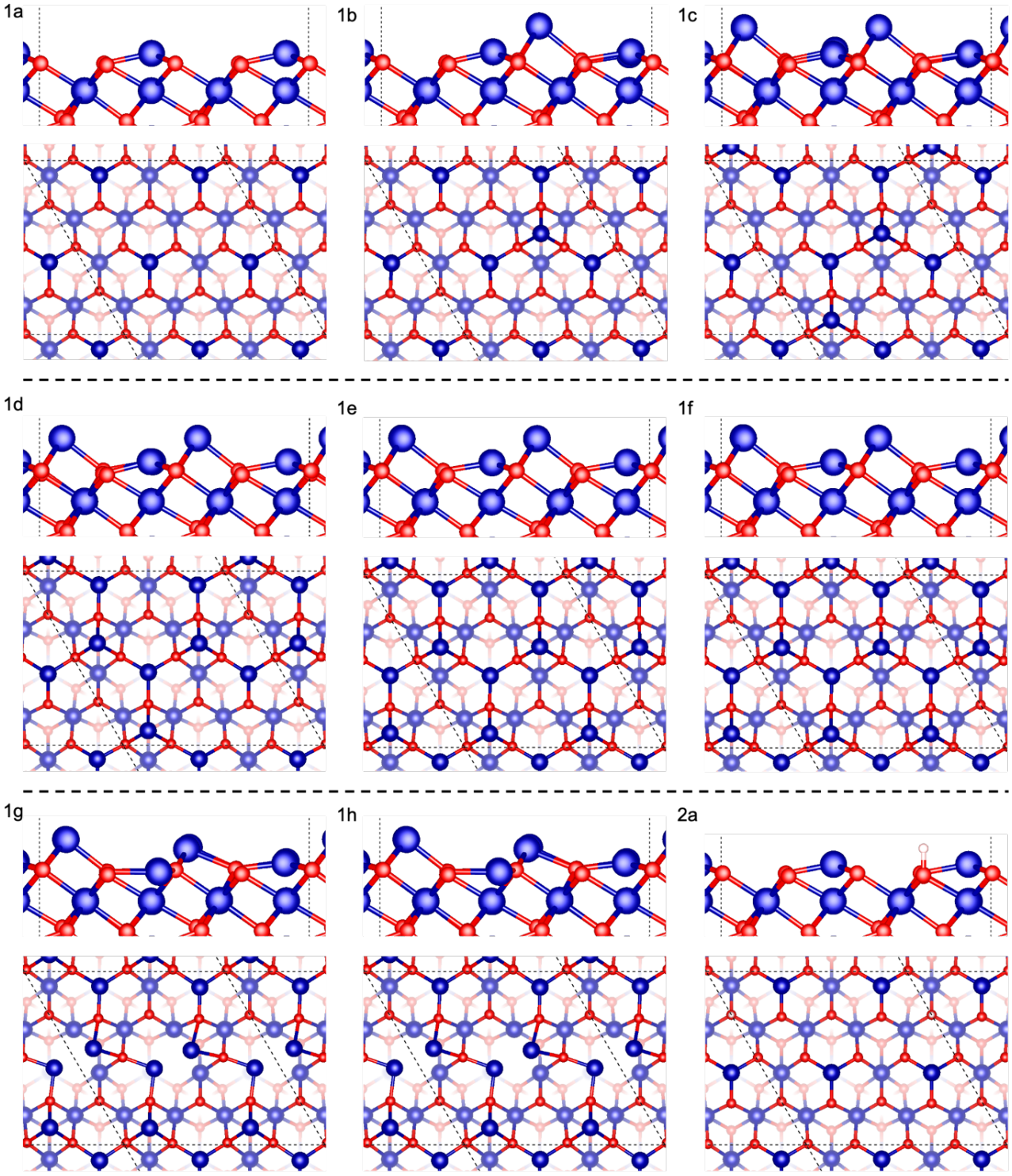

FIG. S1: Top and side view of different $Co_3O_4(111)$ surface structures in regions 1a–2a in the phase and Pourbaix diagrams.

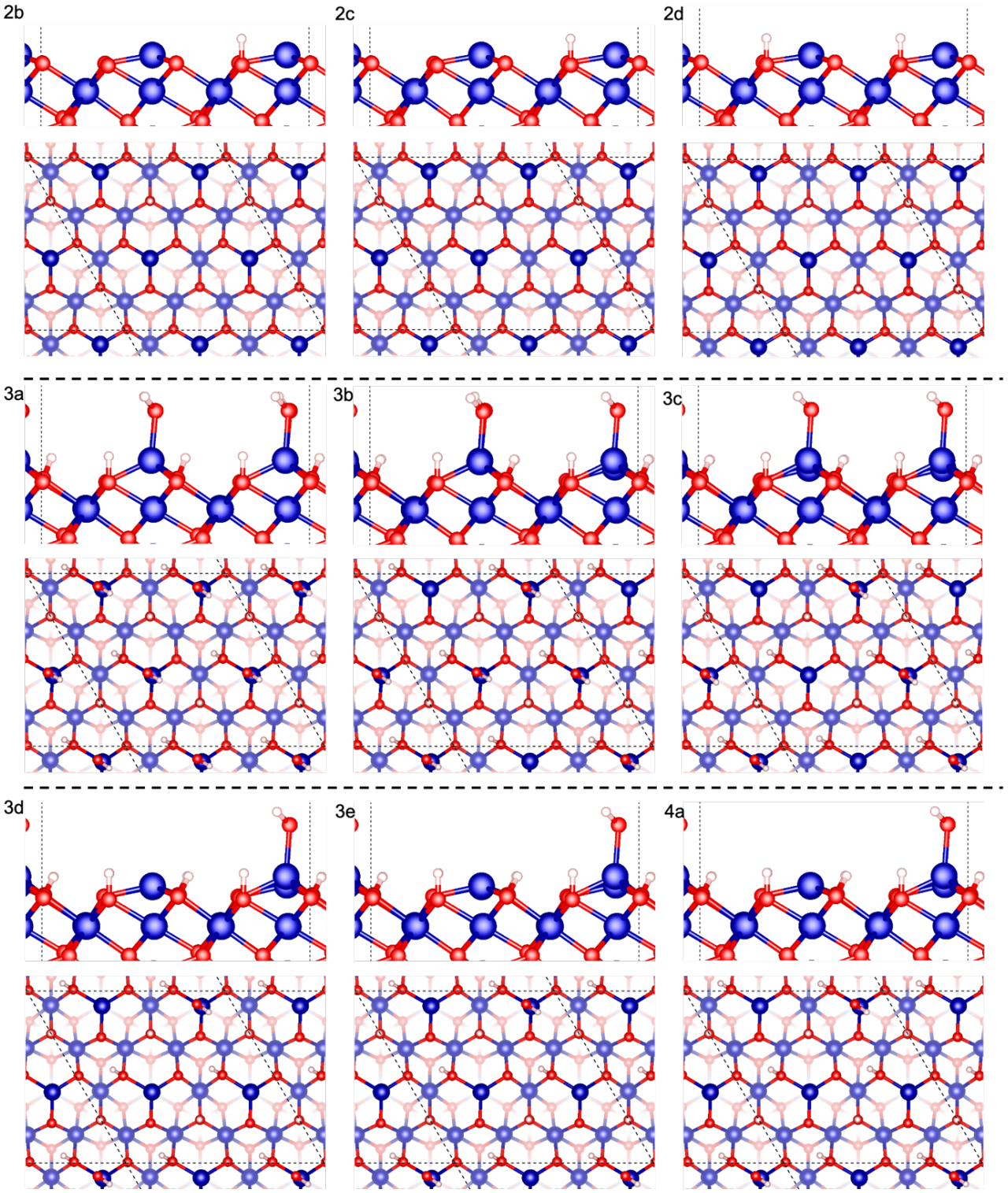

FIG. S2: Top and side view of different $Co_3O_4(111)$ surface structures in regions 2b–4a in the phase and Pourbaix diagrams.

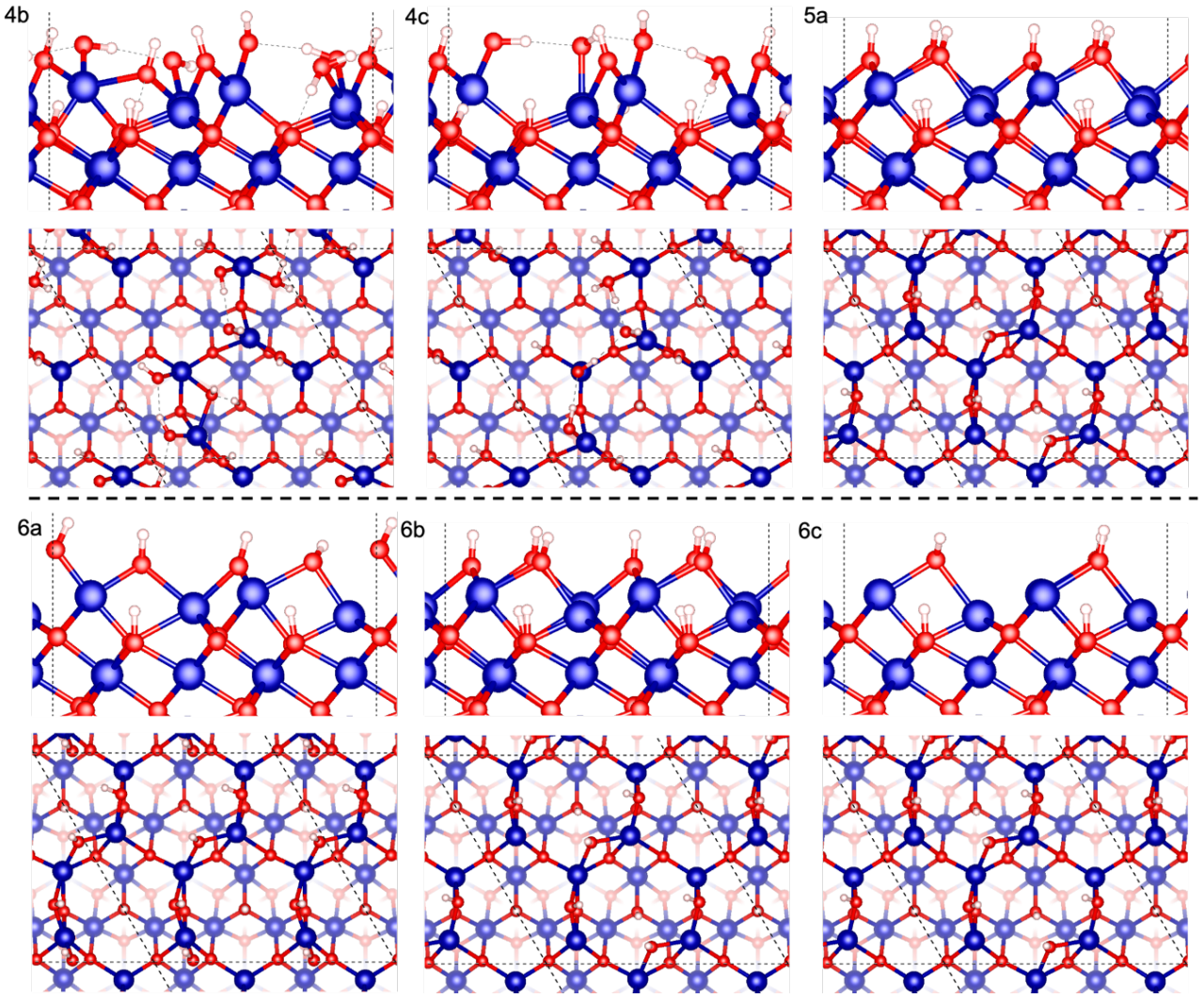

FIG. S3: Top and side view of different $Co_3O_4(111)$ surface structures in regions 4b–6c in the phase and Pourbaix diagrams.

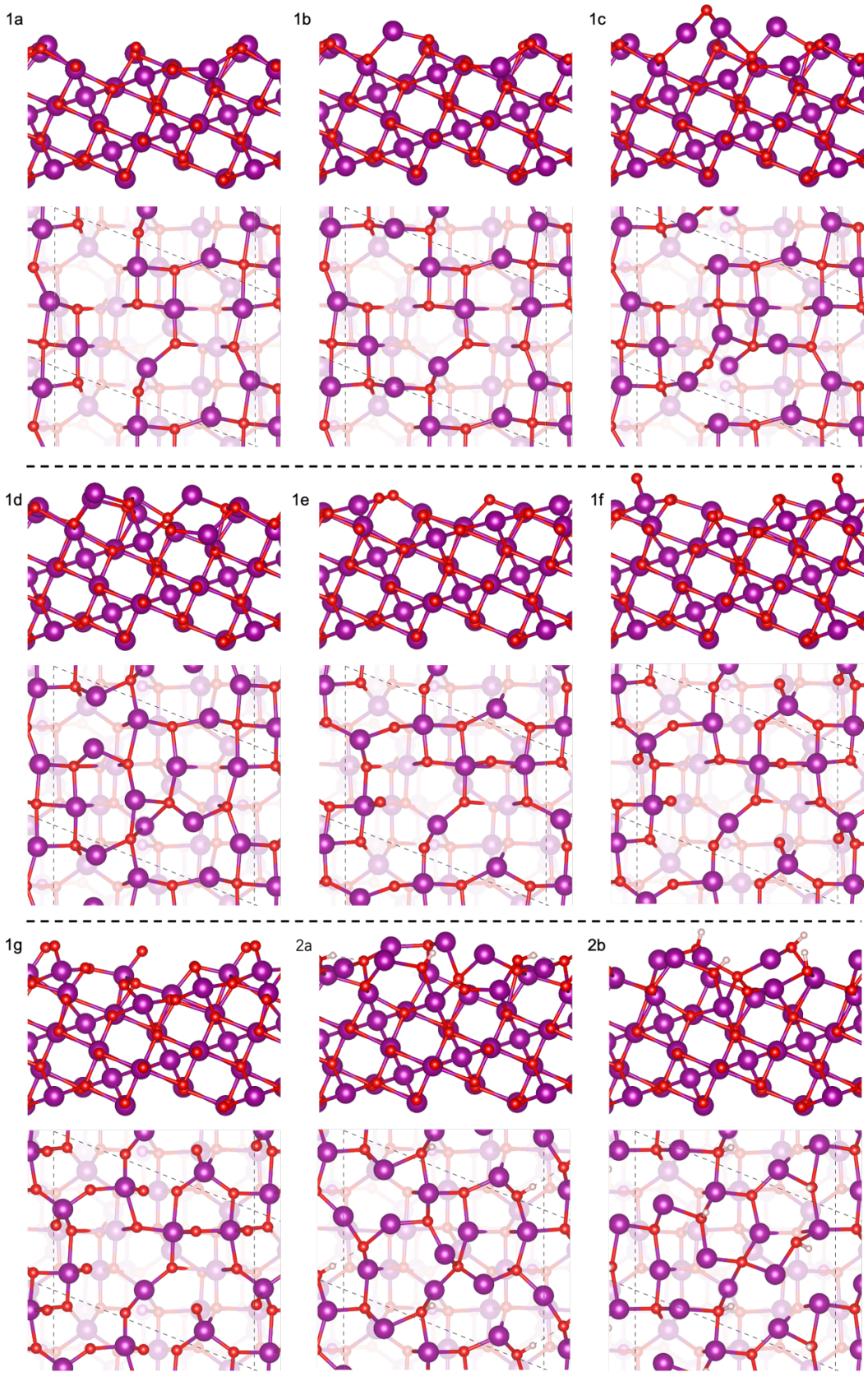

FIG. S4: Top and side view of different $Mn_3O_4(111)$ surface structures in regions 1a–2b in the phase and Pourbaix diagrams.

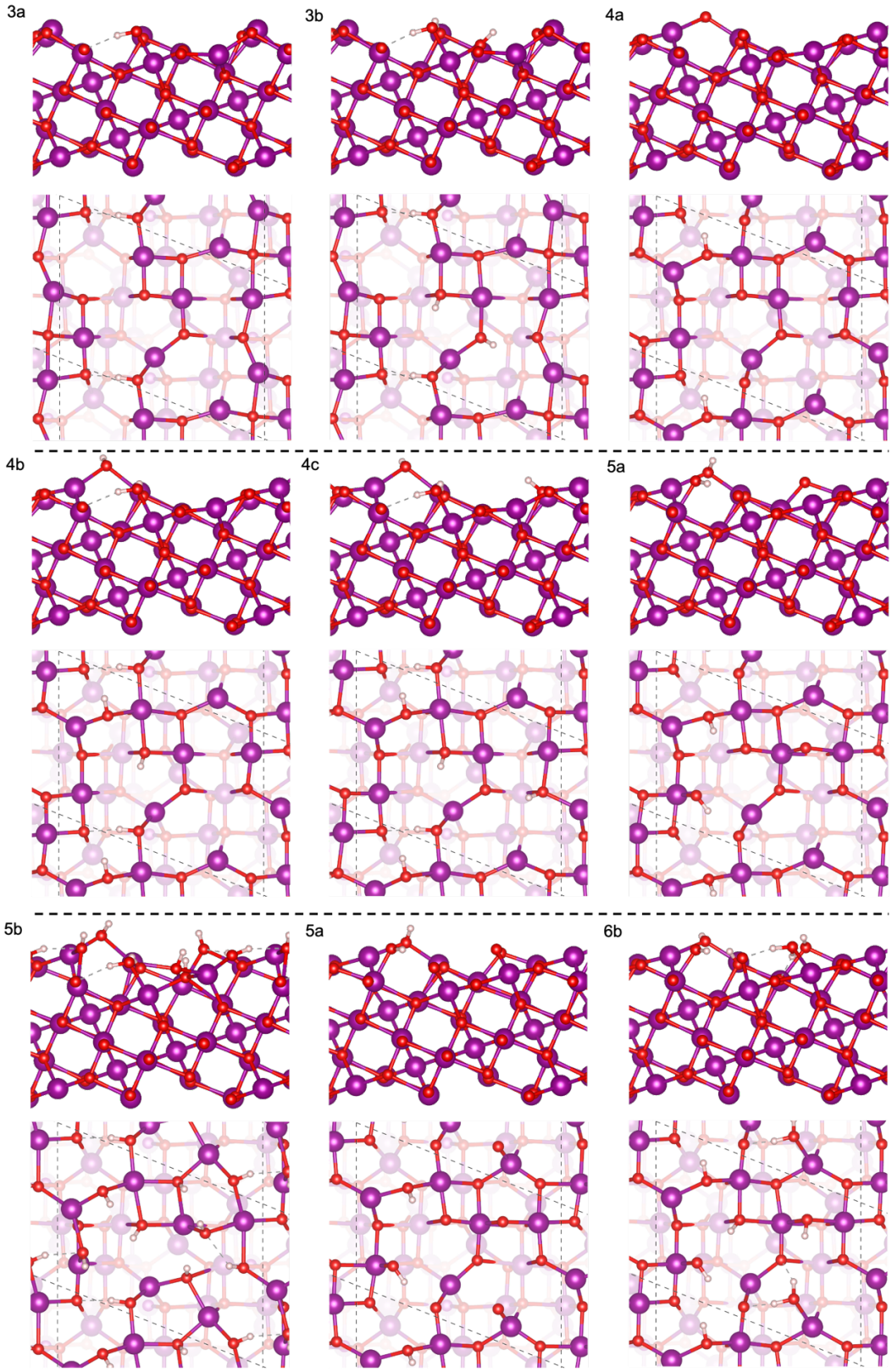

FIG. S5: Top and side view of different $Mn_3O_4(111)$ surface structures in regions 3a–6b in the phase and Pourbaix diagrams.

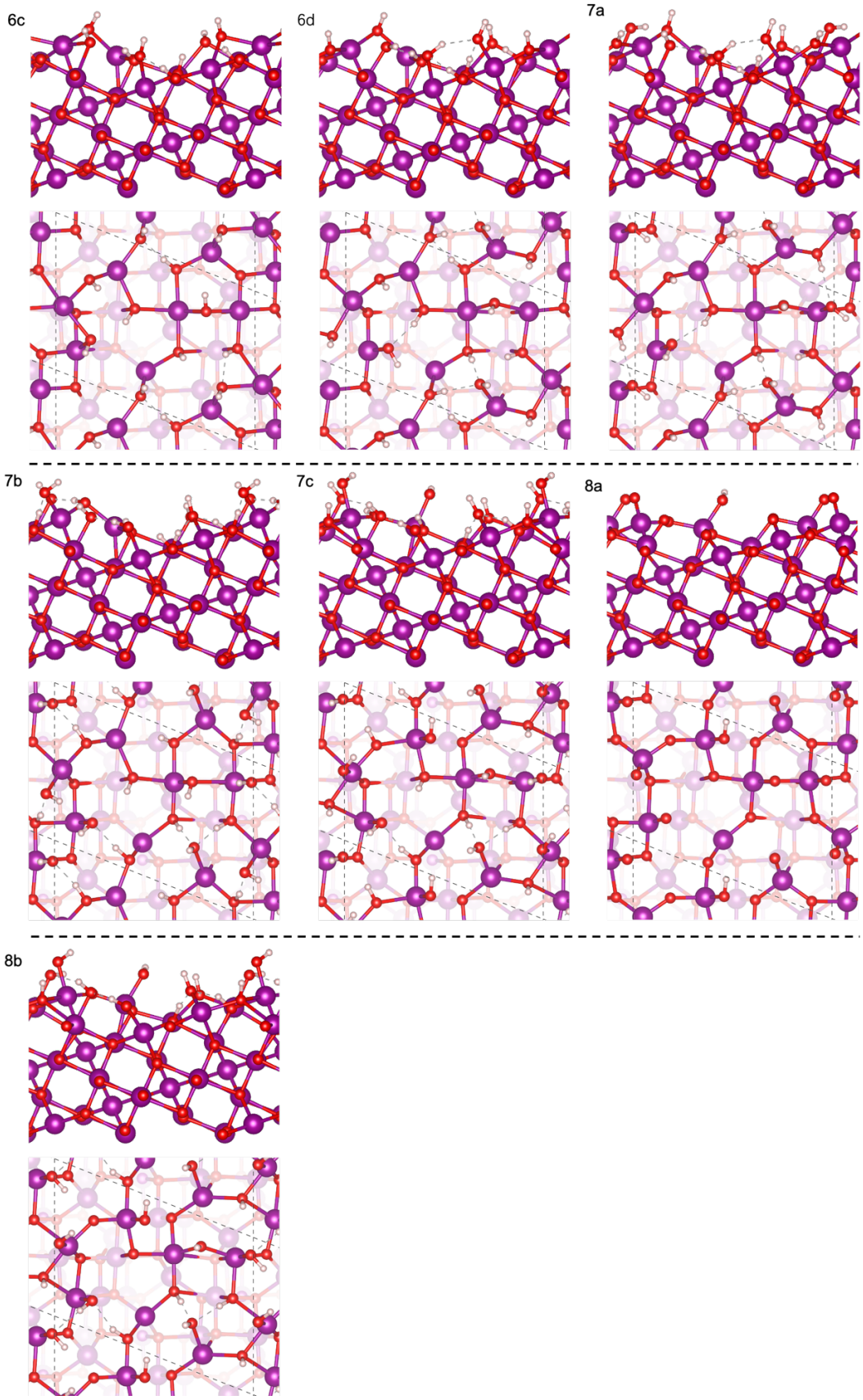

FIG. S6: Top and side view of different $Mn_3O_4(111)$ surface structures in regions 6c–8b in the phase and Pourbaix diagrams.

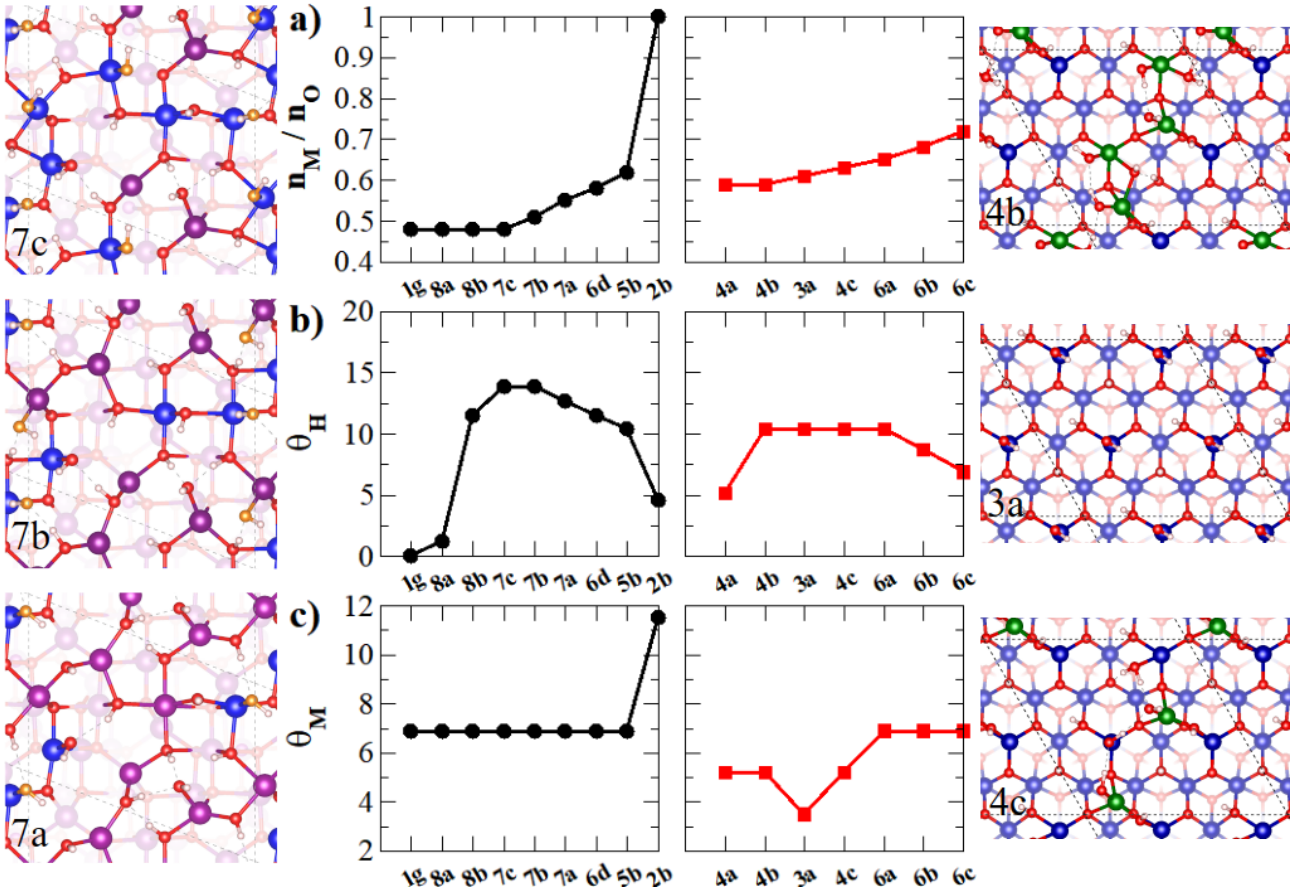

FIG. S7: (a) Proportion of metal to oxygen ions n_M/n_O, amount of (b) adsorbed hydrogen and (c) metal ions per surface area on the most stables Mn_3O_4 (left) and Co_3O_4 (right) (111) surface terminations. Side views of the most relevant systems were added on the sides. Mn^{2+}, Mn^{3+}, Co^{2+}, Co^{3+}, O and H are represented as purple, blue, navy blue, green, red, and white spheres, respectively.

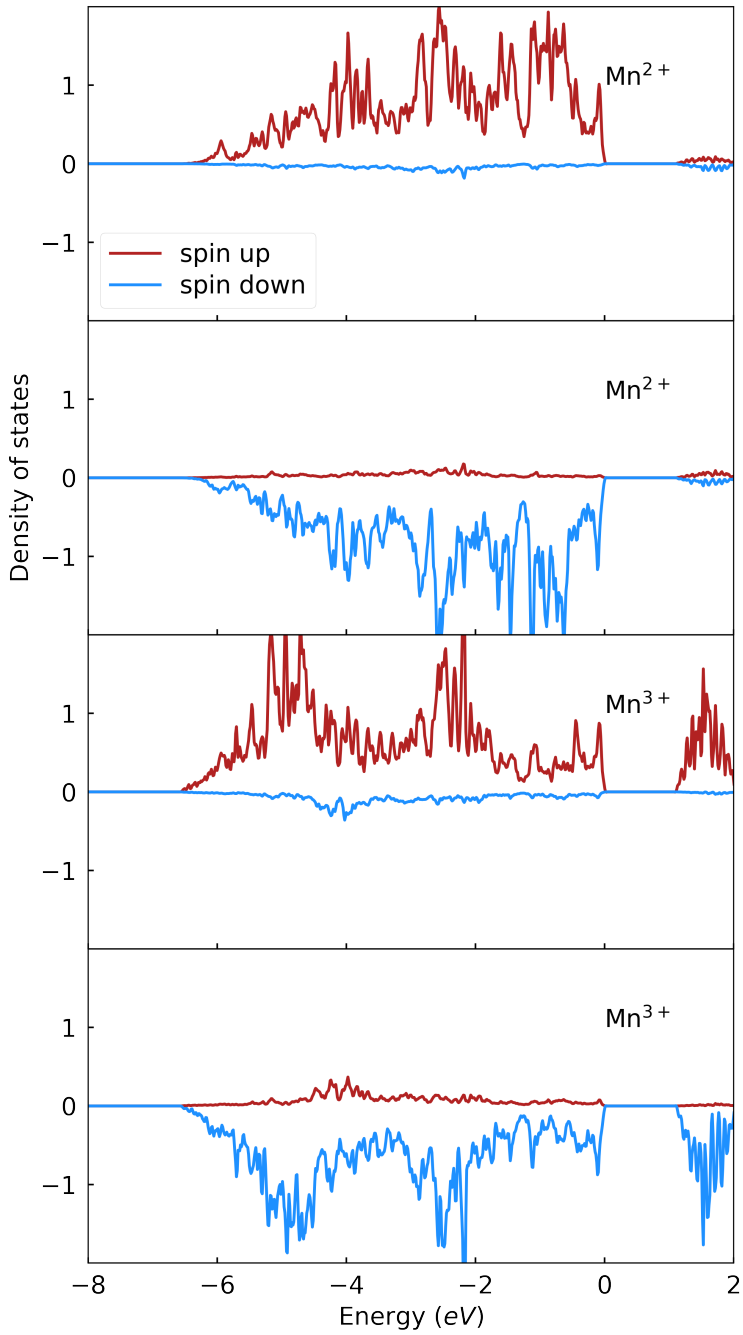

FIG. S8: Projected DOS on the d-band orbitals of Mn_3O_4 bulk. The position of the Fermi level is 0.

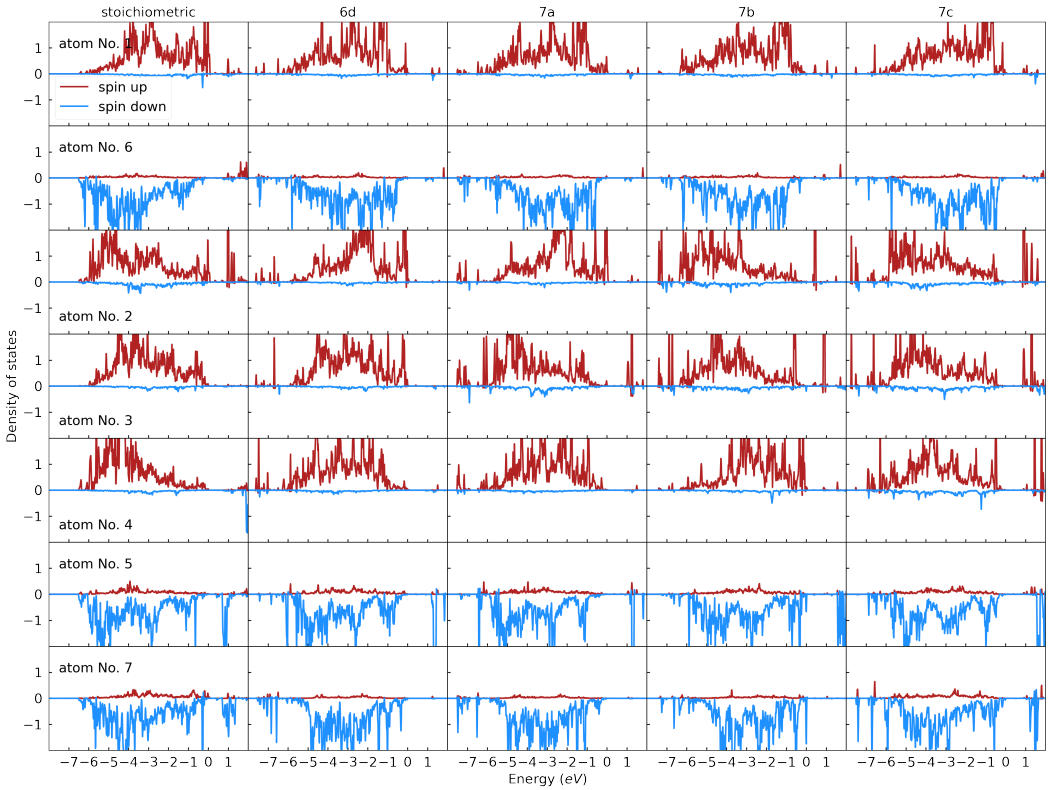

FIG. S9: Projected DOS on the d-band orbitals of different terminations of $Mn_3O_4(111)$ surface. The atoms are labelled according to Figure 8. The position of the Fermi level is 0.